The sigma meson from lattice QCD with two-pion interpolating operators

Dean Howarth and Joel Giedt
Department of Physics, Applied Physics and Astronomy
Rensselaer Polytechnic Institute, 110 8th Street, Troy, NY 12180 USA

Abstract

In this article we describe our studies of the sigma meson, $f_0(500)$, using two-pion correlation functions. We use lattice quantum chromodynamics in the quenched approximation with so-called clover fermions. By working at unphysical pion masses we are able to identify a resonance with mass less than $2m_\pi$, and then extrapolate to the physical point. We include the most important annihilation diagram, which is "partially disconnnected" or "single annihilation." Because this diagram is quite expensive to compute, we introduce a somewhat novel technique for the computation of all-to-all diagrams, based on momentum sources and a truncation in momentum space. In practice, we use only $\mathbf{p} = 0$ modes, so the method reduces to wall sources. At the point where the mass of the pion takes its physical value, we find a resonance in the 0^{++} two-pion channel with a mass of approximately 609 ± 80 MeV, consistent with the expected properties of the sigma meson, given the approximations we are making.

1 Motivation

Scalar resonances in quantum chromodynamics (QCD) have proven to be challenging objects to study in terms of experimental observation, computational studies, and theoretical explanation. The most elusive of these scalar states are arguably the $f_0(500)$ or σ resonance, and the lightest scalar meson with nonzero strangeness, the $\kappa(900)$. As far as the $I = 0$ state is concerned, many experiments over the years have found a broad enhancement in the two-pion spectrum, beginning at threshold and continuing to around 900 MeV: for instance a $\pi^- p \to \pi^-\pi^+ n$ experiment at 17 GeV that ran at CERN 1970-1971 [1], $pp \to p_f\pi^0\pi^0 p_s$ at 450 GeV by the GAMS NA12/2 collaboration also at CERN [2], $\pi^- p \to \pi^0\pi^0 n$ at 18.3 GeV by the Brookhaven E852 experiment [3], and $J/\psi \to \omega\pi^+\pi^-$ by BES II [4]. If anything, the quality of the data has improved over time revealing that the enhancement takes on the shape of a very broad peak centered at around 500 MeV with a comparable width—though the shape may also have something to do with the channel in which the two-pion invariant mass was explored. Also over the years, there have been several lattice calculations of scalar correlation functions in the $I = 0$ $J^{PC} = 0^{++}$ channel, but many of them do not include annihilation diagrams that couple to the vacuum (see for instance Figs. 1(b) and 1(c) below) [5, 6, 7, 8, 9, 10, 11, 12, 13, 14, 15]. Analysis of 0^{++} glueballs in full QCD [16] should also shed light on these states, due to mixing. The LHCb collaboration [17] report that the $f_0(500)$ is not a mesonic bound state according to their models, and present (model dependent) upper limits of the mixing of the $f_0(500)$ between $\bar{u}u + \bar{d}d$ and $\bar{s}s$ constituent quark states. There are several questions that remain open, e.g.,

- The width and mass of the resonance are comparable. While the shape does not agree with the two-pion continuum spectrum, it is possible that strong interaction effects between the two pions could produce such a spectrum, calling into question its identification as a true resonance in the classic sense of the word.

- Though the quantum numbers of the $f_0(500)$ are easy to discern, its partonic content is not known with any degree of confidence. One would certainly expect a large contribution from first generation quarks, and the possibility of contributions from the strange quark are certainly feasible. There is also the question of contributions from purely gluonic states, as yet seen only on the lattice. However, it is usually assumed that this contribution is small since the glueball in quenched lattice QCD has a mass around 1.6 GeV.

- The scattering phase of the two pseudoscalars in this channel ought to shift by π radians if the intermediate state were a coherent and distinct quantum state that behaved like a Breit-Wigner resonance; it is possible that a more general two-meson bound state would give a smaller shift. Confusingly, the 1974 CERN-Munich measurements [18] of this phase shift give an intermediate

value of only $\pi/2$ radians. A possible explanation was offered by Ishida et al. [19] whereby a "repulsive core" in the $f_0(500)$ induces a negative background phase to account for the "missing" phase shift of the channel. However, for a long time this lack of an adequate phase shift has cast doubt on the existence of the $f_0(500)$. Subsequent fits such as [20, 21] have seemingly alleviated this problem, apparently by avoiding the assumption of a Breit-Wigner type phase shift.

- There are also indirect uncertainties about the $f_0(500)$ in the context of its role in a scalar nonet [22, 23] and also a chiral scalar nonet [24]. The $f_0(500)$ can also play the role of a 'Higgs boson' in the context of lightest pseudoscalar mesons being the Nambu-Goldstone bosons of a (broken) chiral symmetry. This idea can be extended to "walking technicolor" models whereby the longitudinal components of the electroweak gauge bosons ($W^{\pm}$, Z^0) are described as composite particles known as techni-pions composed of techni-quarks. In fact, the Higgs boson has even been proposed as the pseudo-Nambu-Goldstone boson of scale invariance (see [25] for a review). So one wonders whether there is any connection between $f_0(500)$ and scale invariance in QCD.[1]

Lattice QCD can shed light on some of these matters from a model independent, *ab initio* perspective. By identifying the $f_0(500)$ state on the lattice, we can measure its mass and other properties using well established techniques. Once this is done, we can use Lüscher's method to measure the $I = 0$, $L = 0$ scattering phase shift δ_0^0 of the $\pi^+\pi^- \to \pi^+\pi^-$ system. This measurement has the benefit of not requiring a partial wave analysis with several intermediate states fit simultaneously, as is necessary in the experimental approach. In the calculation presented here, we show how the ground state energy of the $\pi^+\pi^- \to \pi^+\pi^-$ system at six different pion masses evolves with bare quark mass m_0 and that a linear extrapolation of these masses to physical scales indicates that the observed ground state is that of the $f_0(500)$. Given that the principal decay of the σ is probably to $\pi\pi$ states, it seems that there should be a strong coupling to the interpolating operators that we use. It is also suggested by the tetraquark proposal for this state [26, 27]. Our work is quite similar to [8], including working at heavy pion masses where the resonance lies below $2m_\pi$. Here, however we include the partially disconnected (single annihilation) diagrams, Figs. 1(c) and 1(d).

2 The four-point pseudoscalar correlation function

In order to study a 0^{++} scalar state such as the $f_0(500)$ we must create a state on the lattice with the same quantum numbers. One such state is $\pi^+\pi^-$ which we can create by inserting pseudoscalar creation operators $P^{+\dagger}$ and $P^{-\dagger}$ at at $(\mathbf{0}, 0)$ and

[1] Of course scale invariance is badly broken in QCD due to the quark masses and the scale anomaly, due to a relatively large β function.

($\mathbf{x}$,0) respectively. We then destroy the pseudoscalars at ($\mathbf{y}$,t) and ($\mathbf{z}$,t), leading to the correlation function

$$C(t) = \langle \Omega | T\{P^-(\mathbf{z},t)P^+(\mathbf{y},t)P^{-\dagger}(\mathbf{x},0)P^{+\dagger}(\mathbf{0},0)\}|\Omega\rangle, \tag{1}$$

where in terms of the quark fields

$$\begin{aligned} P^{+\dagger}(\mathbf{x},t) &= \bar{u}(\mathbf{x},t)\gamma_5 d(\mathbf{x},t), \\ P^{-\dagger}(\mathbf{x},t) &= \bar{d}(\mathbf{x},t)\gamma_5 u(\mathbf{x},t). \end{aligned} \tag{2}$$

For notational convenience we work with the understanding that the points y and z are located at timeslice $t \geq 0$, and x and 0 are located at $t_0 = 0$. After performing the relevant Wick contractions there are four distinct propagator diagrams, illustrated in Fig. 1. We subtract from each relevant correlation function the (truly) disconnected pieces to leave only the truly connected part and average over gauge field configurations.[2]

Since we are calculating $\pi^+\pi^- \to \pi^+\pi^-$ with zero momentum pions, both $I = 0$ and $I = 2$ channels with $I_3 = 0$ contribute. However, based on the result of [8], as well as what is known experimentally, we do not expect a resonance in the $I = 2$ channel for the 0^{++} states. Thus the resonant feature that we are able to observe in our simulations is to be identified with an $I = 0$ hadron, such as $f_0(500)$, $f_0(980)$ or $f_0(1370)$. We also avoid the "crossed" or "quark exchange" diagrams that occur in $\pi^0\pi^0 \to \pi^0\pi^0$, which is necessary to include if an $I = 0$ projection is performed (see for instance Fig. 1(b) of [28] where such diagrams were included).

We wish to measure the ground state energy of the system, so we at this point project the pseudoscalar operators onto zero momentum.[3] The momentum of the pions $\mathbf{p}$ at each respective lattice point obeys $\mathbf{p}_0 + \mathbf{p}_x = \mathbf{P} = \mathbf{p}_y + \mathbf{p}_z$, hence there are many combinatorial choices of pion momenta that satisfy $\mathbf{P} = 0$. We expect, however, that the choice $\mathbf{p}_x = \mathbf{p}_y = \mathbf{p}_z = 0$ will have a significant overlap with $\mathbf{P} = 0$, especially in the heavy quark limit where one can expect $2m_\pi > 500$ MeV. For lower quark masses, this assumption will be less true. The Fourier transformed correlation

[2] In lattice QCD, diagrams where quark lines are not connected are often called "disconnected" even though the average of the gauge field configurations effectively connects the quark lines through gluon interactions.

[3] Ultimately we will end up projecting the quark fields themselves onto momentum eigenstates.

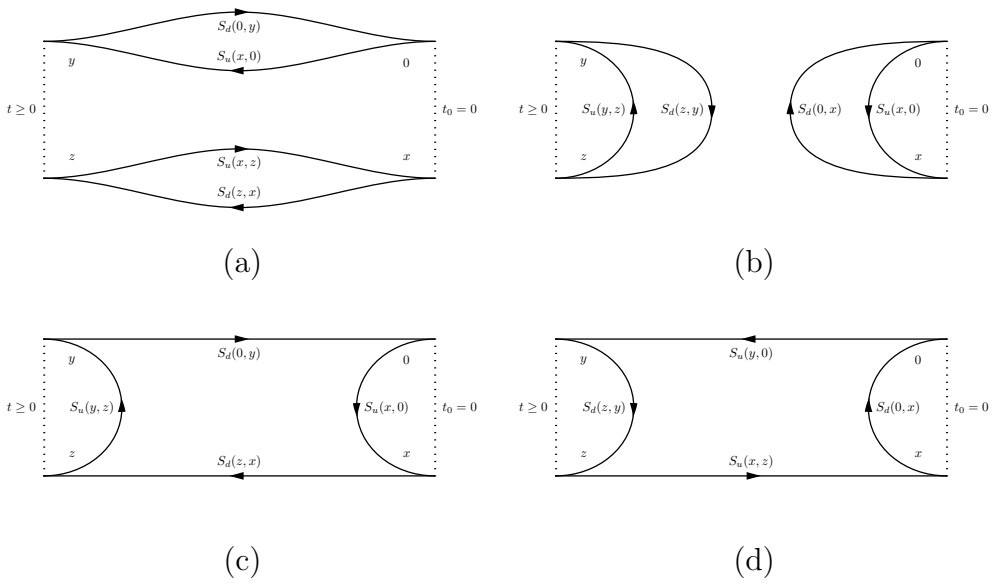

Figure 1: The four types of contractions of the quark fields that we can have. These propagators are then averaged over the gauge field configurations to get the correlation function. Diagrams (a), (b), (c) and (d) correspond to correlation functions C_0, C_1, C_2 and C_3 respectively.

functions $C_n(\mathbf{P} = 0, t)$ are,

$$C_0(\mathbf{0},t) = \left\langle \sum_{\mathbf{x},\mathbf{y},\mathbf{z}} \mathrm{Tr}\big[S(x,z)S^\dagger(x,z)\big]\mathrm{Tr}\big[S(y,0)S^\dagger(y,0)\big] \right\rangle_U - \left\langle \sum_{\mathbf{x},\mathbf{y},\mathbf{z}} \mathrm{Tr}\big[S(x,z)S^\dagger(x,z)\big] \right\rangle_U \left\langle \mathrm{Tr}\big[S(y,0)S^\dagger(y,0)\big] \right\rangle_U , \tag{3a}$$

$$C_1(\mathbf{0},t) = \left\langle \sum_{\mathbf{x},\mathbf{y},\mathbf{z}} \mathrm{Tr}\big[S(y,z)S^\dagger(y,z)\big]\mathrm{Tr}\big[S(x,0)S^\dagger(x,0)\big] \right\rangle_U - \left\langle \sum_{\mathbf{x},\mathbf{y},\mathbf{z}} \mathrm{Tr}\big[S(y,z)S^\dagger(y,z)\big] \right\rangle_U \left\langle \mathrm{Tr}\big[S(x,0)S^\dagger(x,0)\big] \right\rangle_U , \tag{3b}$$

$$C_2(\mathbf{0},t) = \left\langle \sum_{\mathbf{x},\mathbf{y},\mathbf{z}} \mathrm{Tr}\big[S(y,z)S^\dagger(x,z)S(x,0)S^\dagger(y,0)\big] \right\rangle_U , \tag{3c}$$

$$C_3(\mathbf{0},t) = \left\langle \sum_{\mathbf{x},\mathbf{y},\mathbf{z}} \mathrm{Tr}\big[S(x,z)S^\dagger(y,z)S(y,0)S^\dagger(x,0)\big] \right\rangle_U , \tag{3d}$$

where $S(x,z)$ is the Euclidean quark propagator from z to x and the trace is over spin

and colour indices, which have been suppressed. The notation $\langle \cdots \rangle_U$ indicates an average over gauge fields. We have imposed u, d quark mass degeneracy and employed γ_5-hermiticy,

$$S(x,z) = \gamma_5 S^\dagger(z,x)\gamma_5, \tag{4}$$

which eliminates the γ_5 matrices in the pseudoscalar operators. The full correlation function $C_{\rm sum}(\mathbf{P}=0,t)$ is given by,

$$C_{\rm sum}(\mathbf{0},t) = C_0(\mathbf{0},t) + C_1(\mathbf{0},t) - 2\,{\rm Re}\; C_2(\mathbf{0},t), \tag{5}$$

as $C_3(\mathbf{0},t)$ is the complex conjugate of $C_2(\mathbf{0},t)$.

The correlation function can also be represented as the sum of exponentials of energy E_n,

$$C_{\rm sum}(\mathbf{P},t) = \sum_n A_n(\mathbf{P}) e^{-E_n(\mathbf{P})t}, \qquad E_0 < E_1 < E_2 < .... \tag{6}$$

In the limit of $t \to \infty$, the correlation function will be dominated by the lowest energy level. By defining an effective mass,

$$\begin{aligned} m_{\rm eff}(\mathbf{P},t) &= -\ln\left[\frac{C_{\rm sum}(\mathbf{P},t+1)}{C_{\rm sum}(\mathbf{P},t)}\right] \\ \lim_{t\to\infty} m_{\rm eff} &= (\mathbf{P},t)E_0, \end{aligned} \tag{7}$$

we can extract the ground state of any resonance that lies below $2m_\pi$.

3 Quark propagator approximation with smeared wall sources

As can be seen from Eqs. (3), one needs to place quark sources at 0 and z, and sink the quark propagators at x and y. The propagators sourced at 0 are very cheap as we can use a point source and need only calculate them once per gauge field configuration. The propagators sourced at z require considerable computational effort to calculate if one is to project the pseudoscalar at z to zero momentum. If one were to employ point sources, one would have to invert the associated fermion matrix M an entire Euclidian spacetime volume's worth of times (or some significant fraction thereof) which is prohibitive on larger lattices. One solution is to estimate the propagators using stochastic sources, as is done elegantly in [29], or a more sophisticated technique such as the Laplace-Heaviside method [30] or even an amalgam of both [31]. Each of these techniques offer a substantial reduction in the number of inversions required to calculate sufficiently accurate propagators.

3.1 Momentum sources

Another method is to use momentum sources, such as used by Gockeler et al. in [32, 33], which are unit wall sources (defined only on one time slice) and modulated by a momentum phase,

$$\rho_{\mathbf{p}}(\mathbf{x},t) = e^{i\mathbf{p}\cdot\mathbf{x}}\rho(\mathbf{x},t), \tag{8}$$

where $\rho(\mathbf{x},t)$ is unit valued at all $\mathbf{x}$ for a given t. The sources form a complete set when summed over all $\mathbf{p}$ and one can form the component of the full all-to-all propagator which is sourced at t. This is in complete analogy with stochastic sources expressed as column vectors $\eta_i(x)$, where one exploits the conditions,

$$\lim_{N\to\infty}\frac{1}{N}\sum_{i=0}^{N-1}\eta_i(x)\eta_i(y)^\dagger = \delta(x,y), \qquad \lim_{N\to\infty}\frac{1}{N}\sum_{i=0}^{N-1}\eta_i(x) = 0, \tag{9}$$

to solve a simple, linear matrix-vector system for $\phi_i(x)$ and build the approximate propagator after summing over many distinct $\eta_i(x)$,

$$\begin{aligned}
\phi_i(y) &= M^{-1}(y;x)\eta_i(x), \\
\frac{1}{N}\sum_{i=0}^{N-1}\phi_i(x)\eta_i(y)^\dagger &= \frac{1}{N}\sum_{i=0}^{N-1}M^{-1}(x;z)\eta_i(z)\eta_i(y)^\dagger, \\
\lim_{N\to\infty}\frac{1}{N}\sum_{i=0}^{N-1}\phi_i(x)\eta_i(y)^\dagger &= M^{-1}(x;y).
\end{aligned} \tag{10}$$

In the case of momentum sources, one need only sum over the finite range of distinct momentum modes $\mathbf{p}$ per timeslice to acquire an approximation to the full propagator. The procedure is strikingly similar,

$$\frac{1}{V_P}\sum_{\mathbf{p}\in P}\rho_{\mathbf{p}}(x)\rho_{\mathbf{p}}(y)^\dagger = \frac{1}{V_P}\sum_{\mathbf{p}\in P}\rho(x)\rho(y)^\dagger e^{-i\mathbf{p}\cdot(\mathbf{y}-\mathbf{x})} = \delta(x,y), \qquad \frac{1}{V_P}\sum_{\mathbf{p}\in P}\rho_{\mathbf{p}}(x) = 0, \tag{11}$$

where P is all allowed momenta and V_P a Fourier normalisation factor. Then, for some $\chi_{\mathbf{p}}(x)$,

$$\begin{aligned}
\chi_{\mathbf{p}}(y) &= M^{-1}(y;x)\rho_{\mathbf{p}}(x), \\
\frac{1}{V_P}\sum_{\mathbf{p}\in P}\chi_{\mathbf{p}}(x)\rho_{\mathbf{p}}(y)^\dagger &= \frac{1}{V_P}\sum_{\mathbf{p}\in P}M^{-1}(x;z)\rho_{\mathbf{p}}(z)\rho_{\mathbf{p}}(y)^\dagger, \\
\frac{1}{V_P}\sum_{\mathbf{p}\in P}\chi_{\mathbf{p}}(x)\rho_{\mathbf{p}}(y)^\dagger &= M^{-1}(x;y).
\end{aligned} \tag{12}$$

Of course, summing over all possible momentum modes would be just as computationally expensive as summing over all point sources. However, we might reasonably expect that some subset of the low momenta have good overlap with the low energy component of the full propagator. If we restrict that subset to momenta that satisfy,

$$\left| \frac{2}{a} \sin\left(\frac{\mathbf{p}a}{2}\right) \right| \ll \frac{1}{a} \tag{13}$$

for some lattice spacing a, and denote that subset as Q, the we can 'project' the propagator onto those low modes,

$$\begin{aligned} \frac{1}{V_Q} \sum_{\mathbf{p}\in Q} \chi_{\mathbf{p}}(x)\rho_{\mathbf{p}}(y)^\dagger &= \frac{1}{V_Q} \sum_{\mathbf{p}\in Q} M^{-1}(x;z)\rho_{\mathbf{p}}(z)\rho_{\mathbf{p}}(y)^\dagger, \\ &\equiv M_Q^{-1}(x;y). \end{aligned} \tag{14}$$

Furthermore, the contribution to the correlation function coming from high momentum modes is suppressed for the ground states that we explore so it is a reasonable approximation to cut off the propagator in this way. However, this truncation is not a gauge covariant procedure; for this reason we have averaged over typically 4,000 gauge field configurations so that the gauge variant part will cancel to a good approximation. Performing gauge fixing may have improved the signal-to-noise ratio, but would not change the central value, which is the gauge invariant part. We found that such gauge fixing was not necessary.

For our current investigation, the least expensive subset Q is of course the one that only contains the zero momentum mode. This is nothing other that the method of wall sources. In this respect, using the $\mathbf{p} = 0$ momentum mode at z and 0 in our calculation is the momentum space analogue of a point-to-all propagator. The advantage with the wall source is that it automatically projects onto total momentum $\mathbf{P} = 0$ for the two-pion operators, once the appropriate Fourier transform at the sink is performed.

With this in mind, we may re-express the correlation functions defined in equations (3) in terms of propagators with mixed position- and momentum-space structure, $S(x, \mathbf{0})$ to reflect the projection of the pseudoscalars sourced at z and 0 to zero

momentum,

$$C_0(\mathbf{0},t) = \left\langle \sum_{\mathbf{x},\mathbf{y}} \mathrm{Tr}\big[S(x,\mathbf{0})S^\dagger(x,\mathbf{0})\big]\mathrm{Tr}\big[S(y,\mathbf{0})S^\dagger(y,\mathbf{0})\big] \right\rangle_U - \left\langle \sum_{\mathbf{x},\mathbf{y}} \mathrm{Tr}\big[S(x,\mathbf{0})S^\dagger(x,\mathbf{0})\big] \right\rangle_U \left\langle \mathrm{Tr}\big[S(y,\mathbf{0})S^\dagger(y,\mathbf{0})\big] \right\rangle_U , \tag{15a}$$

$$C_1(\mathbf{0},t) = \left\langle \sum_{\mathbf{x},\mathbf{y}} \mathrm{Tr}\big[S(y,\mathbf{0})S^\dagger(y,\mathbf{0})\big]\mathrm{Tr}\big[S(x,\mathbf{0})S^\dagger(x,\mathbf{0})\big] \right\rangle_U - \left\langle \sum_{\mathbf{x},\mathbf{y}} \mathrm{Tr}\big[S(y,\mathbf{0})S^\dagger(y,\mathbf{0})\big] \right\rangle_U \left\langle \mathrm{Tr}\big[S(x,\mathbf{0})S^\dagger(x,\mathbf{0})\big] \right\rangle_U , \tag{15b}$$

$$C_2(\mathbf{0},t) = \left\langle \sum_{\mathbf{x},\mathbf{y}} \mathrm{Tr}\big[S(y,\mathbf{0})S^\dagger(x,\mathbf{0})S(x,\mathbf{0})S^\dagger(y,\mathbf{0})\big] \right\rangle_U , \tag{15c}$$

$$C_3(\mathbf{0},t) = \left\langle \sum_{\mathbf{x},\mathbf{y}} \mathrm{Tr}\big[S(x,\mathbf{0})S^\dagger(y,\mathbf{0})S(y,\mathbf{0})S^\dagger(x,\mathbf{0})\big] \right\rangle_U . \tag{15d}$$

The summation is now over $\mathbf{x}$ and $\mathbf{y}$ only which saves an order of L^3 in both propagator storage space, and spin-color trace calculation. When employing spin-color-time dilution, this technique requires only $T \times N_{\mathrm{spin}} \times N_{\mathrm{colour}}$ inversions to approximate the low mode propagator, which is a particularly attractive feature.

3.2 Smearing

In order to suppress the effects of excited states, one usually applies a gauge covariant differential function to the quark source to suppress such contributions. For a point source in position space, this has the effect of making the Kronecker-delta distribution representing the point source (the discrete version of the continuum Dirac-delta distribution) and forming a gaussian peak with its mean at the original position of the point source. The effect of this smearing in momentum space can be seen intuitively; the flatter the the gaussian in position space, the sharper the gaussian in momentum space, which means fewer exited modes are populated. A perfectly flat source in position-space corresponds to an ideal "point" source in momentum space, but this will not generate the ground state exactly, but will have overlap with excited states. We applied the Jacobi smearing operator,

$$J^{ab}(\mathbf{x},\mathbf{y}) = \delta_{\mathbf{x},\mathbf{y}}\delta^{a,b} + \frac{\omega^2}{4N}\widetilde{\Delta}^{ab}(\mathbf{x},\mathbf{y}), \tag{16}$$

where the gauge covariant second derivative $\widetilde{\Delta}$ is defined as,

$$\widetilde{\Delta}^{ab}(\mathbf{x},\mathbf{y}) = \sum_{n=1}^{3} \left[U_n^{ab}(\mathbf{x})\delta_{\mathbf{x}+\hat{n},\mathbf{y}} + U_n^{ab\,\dagger}(\mathbf{x}-\hat{n})\delta_{\mathbf{x}-\hat{n},\mathbf{y}} - 2\delta^{a,b}\delta_{\mathbf{x},\mathbf{y}} \right],$$

to the unit wall source with $N = 32, \omega = 4$ to form a smeared momentum source $\widetilde{\rho}^a_{\mathbf{p}}(\mathbf{x})$,

$$J^{ab}(\mathbf{x},\mathbf{y}) e^{i\mathbf{p}\cdot\mathbf{x}} \rho^b(\mathbf{y}) = \widetilde{\rho}^a_{\mathbf{p}}(\mathbf{x}). \tag{17}$$

For the unit wall source at zero momentum, the momentum phase is everywhere unity. This smeared source now has a colour dependency wherein each spatial site inherits information from the surrounding gauge links. The gauge links in the smeared operator were replaced by stout smeared links, with $n = 3$ smearing hits, weighted by the coefficient $\xi_{\mu\nu} = 0.1$ for $\mu = \nu = 1, 2, 3$, and zero elsewhere.

The hopping parameter $\kappa \equiv \omega^2/4N = 0.125$ is a reasonable value when generating gaussian sources from point sources, and for momentum sources we found excellent suppression of excited states in early time slices, for both the C_0 and C_2 diagrams. The C_1 diagram remained very noisy at all but the earliest of time slices. Previous lattice studies on this system opted to omit the contributions from this particular contraction of the quarks in (3) which we were also forced to do as the level of noise from this diagram drowned out all signal. High statistics study show that the C_1 diagram contribution is very small, once the disconnected part is subtracted off. This is because the unsubtracted correlation function is to a very good approximation flat, a result of the operators at the sink and source "disappearing" into the vacuum.

The excited state suppression can be understood in light of v. Hippel et al. [34]. They show that instances of highly localised chromomagnetic flux in the gauge field can distort the shape of a covariantly smeared quark source away from the expected profile. In the present case, the colour diluted, unsmeared momentum sources are themselves a global source of chromomagnetic flux, having a rather unnatural real, unit value in one color vector component and zero elsewhere. This chromomagnetic flux manifests as excited quark modes in the effective mass plot, which then dissipate with t. Application of the smearing operator to the momentum source dampens this effect by sampling the gauge field local to the lattice point and "smoothing" the local chromomagnetic flux with respect to the gauge background.

4 Results

All of the results presented in this section are obtained with gauge coupling of $\beta = 6/g^2 = 5.45$ and clover fermions with the tree-level improvement coefficient of $c_{\mathrm{SW}} = 1.0$. This is a quenched calculation, so the fermion determinant is set to unity in the simulation, which is performed with the standard $SU(3)$ heatbath [35]. 5000

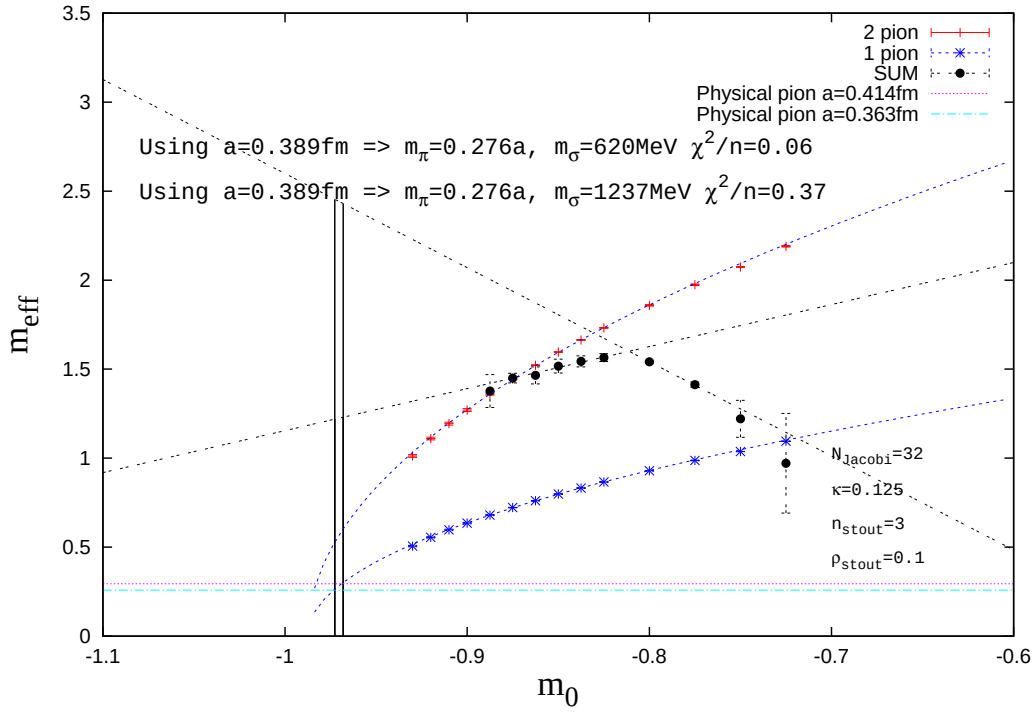

Figure 2: Effective masses, in lattice units, for the four-point correlation function (15) shown in black dots. For comparison, the two-pion mass $2m_\pi$ is plotted with red pluses and the single pion mass with blue splashes (color on-line).

thermalization sweeps were performed prior to sampling, and samples were separated by 200 sweeps. For all but the lightest pion mass, 4000-4500 samples were used in our expectation values. For the lightest mass, only 2000 samples were used. In order to address autocorrelations, the error estimates were based on a jackknife analysis with jackknife blocks of 400 samples. All data was obtained from $10^3 \times 20$ lattices, which is why the coarse lattice spacing corresponding to $\beta = 5.45$ was used ($a \sim 0.4$ fm). For the relatively large pion masses that we simulated, the finite volume effects are under control, with $m_\pi L \geq 4$.

As stated in the previous section, we were forced to omit the $C_1(t)$ contribution from our calculation due to the large amount of noise it introduces. We can expect reasonable results even with this omission as the numerical values of $C_1(t)$ are much larger than the other contributions, but exhibit little to no sign of exponential decay. On the other hand, we do include the partially disconnected diagram $C_2(t)$, which it has been argued in [36] is the most important one to include and should never be neglected.

Figure 2 shows the effective masses derived from the correlation function,

$$C'_{\text{sum}} = C_1(t) - 2C_2(t), \tag{18}$$

for a range of bare quark masses (the prime indicates that the doubly disconnected diagram is omitted). It is straightforward to convert these bare quark masses into pion masses using the single pion correlation function effective mass, which allows us to identify the physical point once the lattice scale a has been set. Three traits can be observed for the effect masses that we see from (18).

1. For the lighest masses, $m_0 = -0.8875, \ldots, -0.875$, the effective mass coincides with $2m_\pi$.

2. For the intermediate masses, $m_0 = -0.8675, \ldots, -0.825$, the effective mass exhibits a linear variation with bare mass. We identify this linear behavior, which is lighter than the corresponding $2m_\pi$, as a scalar state with quantum numbers 0^{++}.

3. For the heavier pion masses, the effective mass diverges from the intermediate mass linear trend, and extrapolates to a much larger mass at the physical point.

We extrapolated the linear behaviour of the intermediate masses down to the physical pion mass, obtaining a mass of 609 ± 80 MeV. This is significantly lighter than the $f_0(980)$, suggesting that the observed state is the $f_0(500)$ or σ. While this is somewhat heavier than the accepted value of 400-550 MeV [37], it is not inconsistent given our estimate of error. Furthermore, there is an unknown systematic error due to quenching (setting the fermion determinant to unity), and it is a large extrapolation, which could also introduce errors that may be unaccounted for. We have also extrapolated the heavier masses and find an interesting result: a mass at

1237 ± 80 MeV. This is not so far from the $f_0(1370)$, and in fact given the unknown quenching uncertainty and extent of the extrapolation, could even correspond to this state.

The physical scale a was deduced by determining the Sommer parameter r_0/a for our value of $\beta = 5.45$ [38]. The exponential decay in Wilson loops with respect to the temporal extent was used to identify the values of the static quark potential $V(R)$. As usual, the Sommer parameter in lattice units was identified from setting $R^2 dV(R)/dR|_{R=r_0/a} = 1.65$ and taking $r_0 = 0.5$ fm to convert to physical units. We use two different prescriptions to identify the plateau, giving two estimates for the lattice spacing. In figure 2 we show these two estimates (0.414 fm and 0.363 fm) but we chose to use their mean to estimate physical mass. A judicious, though *ad hoc* choice of error on this estimate would be to use the separation of the two lattice spacing estimates, giving

$$m_\sigma = 609 \pm 80 \text{ MeV}. \tag{19}$$

This is consistent with a σ to within errors and is not consistent with the other available state in this symmetry channel, the $f_0(980)$. We take encouragement from this exploratory result that the σ can be identified on the lattice.

5 Conclusions and further work

In this work we have shown that with a modest sized, quenched lattice, and a minimum of inversion overhead, one can identify a 0^{++} state that is signficantly lighter than the $f_0(980)$ at physical scales, which one would then naturally identify with the sigma meson. Though we omitted the doubly disconnected diagram contribution $C_1(t)$ we included the singly connected contribution.

We collected this data using a smeared wall source which we identify as an approximation to the gauge-connected zero momentum mode of the source pion. This association allowed us to approximate the zero-mode the all-to-all propagator necessary for this calculation in a very compact fashion, allowing us to calculate the effective mass of several different systems in a reasonable amount of time.

Future studies will repeat the study on larger lattice with a finer lattice spacing, and will also explore the region where the resonance is heavier than $2m_\pi$ by subtracting the two pion scattering state in a sequential Bayesian analysis [39]. We will also explore using the approximation (14) with a subset Q that includes more momentum modes than $\mathbf{p} = 0$.

Acknowledgements

This work was supported in part by NSF Grant No. PHY-1212272. We also benefitted greatly from the use of the Computational Center for Innovation at Rensselaer.

References

[1] G. Grayer, B. Hyams, C. Jones, P. Schlein, P. Weilhammer, et al., *High Statistics Study of the Reaction pi- p –¿ pi- pi+ n: Apparatus, Method of Analysis, and General Features of Results at 17-GeV/c*, *Nucl.Phys.* **B75** (1974) 189.

[2] **GAMS NA12/2** Collaboration, T. Ishida, T. Kinashi, H. Shimizu, K. Takamatsu, and T. Tsuru, *Study of the pi0 pi0 system below 1-GeV region in the p p central collision reaction at 450-GeV/c*, in *Manchester 1995, Proceedings, Hadron '95*, p. 451, 1995.

[3] **E852** Collaboration, J. Gunter et al., *A Partial wave analysis of the pi0 pi0 system produced in pi- p charge exchange collisions*, *Phys.Rev.* **D64** (2001) 072003, [hep-ex/0001038].

[4] **BES** Collaboration, M. Ablikim et al., *The sigma pole in J / psi —¿ omega pi+ pi-*, *Phys.Lett.* **B598** (2004) 149–158, [hep-ex/0406038].

[5] C. E. Detar and J. B. Kogut, *Measuring the Hadronic Spectrum of the Quark Plasma*, *Phys.Rev.* **D36** (1987) 2828.

[6] W.-J. Lee and D. Weingarten, *Scalar quarkonium masses and mixing with the lightest scalar glueball*, *Phys.Rev.* **D61** (2000) 014015, [hep-lat/9910008].

[7] **UKQCD** Collaboration, C. Michael, M. Foster, and C. McNeile, *Flavor singlet pseudoscalar and scalar mesons*, *Nucl.Phys.Proc.Suppl.* **83** (2000) 185–187, [hep-lat/9909036].

[8] M. G. Alford and R. Jaffe, *Insight into the scalar mesons from a lattice calculation*, *Nucl.Phys.* **B578** (2000) 367–382, [hep-lat/0001023].

[9] **UKQCD Collaboration** Collaboration, C. McNeile and C. Michael, *Mixing of scalar glueballs and flavor singlet scalar mesons*, *Phys.Rev.* **D63** (2001) 114503, [hep-lat/0010019].

[10] **SCALAR Collaboration** Collaboration, T. Kunihiro et al., *Scalar mesons in lattice QCD*, *Phys.Rev.* **D70** (2004) 034504, [hep-ph/0310312].

[11] **UKQCD Collaboration** Collaboration, A. Hart, C. McNeile, C. Michael, and J. Pickavance, *A Lattice study of the masses of singlet 0++ mesons*, *Phys.Rev.* **D74** (2006) 114504, [hep-lat/0608026].

[12] S. Prelovsek and D. Mohler, *A Lattice study of light scalar tetraquarks*, *Phys.Rev.* **D79** (2009) 014503, [arXiv:0810.1759].

[13] S. Prelovsek, T. Draper, C. B. Lang, M. Limmer, K.-F. Liu, et al., *Lattice study of light scalar tetraquarks with $i = 0, 2, 1/2, 3/2$: Are σ and κ tetraquarks?*, *Phys.Rev.* **D82** (2010) 094507, [arXiv:1005.0948].

[14] G. P. Engel, C. Lang, M. Limmer, D. Mohler, and A. Schafer, *QCD with two light dynamical chirally improved quarks: Mesons*, *Phys.Rev.* **D85** (2012) 034508, [arXiv:1112.1601].

[15] M. Wakayama, *Structure of the sigma meson from lattice QCD*, *PoS* **Hadron2013** (2014) 106.

[16] **TXL, TkL** Collaboration, G. Bali et al., *Glueballs and string breaking from full QCD*, *Nucl.Phys.Proc.Suppl.* **63** (1998) 209–211, [hep-lat/9710012].

[17] **LHCb** Collaboration, R. Aaij et al., *Measurement of the resonant and CP components in $\overline{B}^0 \to J/\psi\pi^+\pi^-$ decays*, *Phys.Rev.* **D90** (2014), no. 1 012003, [arXiv:1404.5673].

[18] B. Hyams, C. Jones, P. Weilhammer, W. Blum, H. Dietl, et al., *$\pi\pi$ Phase Shift Analysis from 600-MeV to 1900-MeV*, *Nucl.Phys.* **B64** (1973) 134–162.

[19] T. Ishida, *On Existence of sigma (555) particle: Study in p p central collision reaction and reanalysis of pi pi scattering phase shift*, .

[20] F. Yndurain, R. Garcia-Martin, and J. Pelaez, *Experimental status of the pi pi isoscalar S wave at low energy: f(0)(600) pole and scattering length*, *Phys.Rev.* **D76** (2007) 074034, [hep-ph/0701025].

[21] I. Caprini, *Finding the sigma pole by analytic extrapolation of pi pi scattering data*, *Phys.Rev.* **D77** (2008) 114019, [arXiv:0804.3504].

[22] S. Okubo, *Phi meson and unitary symmetry model*, *Phys.Lett.* **5** (1963) 165–168.

[23] G. Zweig, *An SU(3) model for strong interaction symmetry and its breaking. Version 2*, .

[24] M. Ishida, *Possible classification of the chiral scalar sigma nonet*, *Prog.Theor.Phys.* **101** (1999) 661–669, [hep-ph/9902260].

[25] K. Yamawaki, *Conformal Higgs, or techni-dilaton- composite Higgs near conformality*, *Int.J.Mod.Phys.* **A25** (2010) 5128–5144, [arXiv:1008.1834].

[26] R. L. Jaffe, *Multi-Quark Hadrons. 1. The Phenomenology of (2 Quark 2 anti-Quark) Mesons*, *Phys.Rev.* **D15** (1977) 267.

[27] R. L. Jaffe, *Multi-Quark Hadrons. 2. Methods*, *Phys.Rev.* **D15** (1977) 281.

[28] R. Gupta, A. Patel, and S. R. Sharpe, *$I = 2$ pion scattering amplitude with Wilson fermions*, *Phys.Rev.* **D48** (1993) 388–396, [hep-lat/9301016].

[29] J. Foley, K. Jimmy Juge, A. O'Cais, M. Peardon, S. M. Ryan, et al., *Practical all-to-all propagators for lattice QCD*, *Comput.Phys.Commun.* **172** (2005) 145–162, [hep-lat/0505023].

[30] **Hadron Spectrum** Collaboration, M. Peardon et al., *A Novel quark-field creation operator construction for hadronic physics in lattice QCD*, *Phys.Rev.* **D80** (2009) 054506, [arXiv:0905.2160].

[31] C. Morningstar, J. Bulava, J. Foley, K. J. Juge, D. Lenkner, et al., *Improved stochastic estimation of quark propagation with Laplacian Heaviside smearing in lattice QCD*, *Phys.Rev.* **D83** (2011) 114505, [arXiv:1104.3870].

[32] M. Gockeler, R. Horsley, H. Oelrich, H. Perlt, P. E. Rakow, et al., *Lattice renormalization of quark operators*, *Nucl.Phys.Proc.Suppl.* **63** (1998) 868–870, [hep-lat/9710052].

[33] M. Gockeler, R. Horsley, H. Oelrich, H. Perlt, D. Petters, et al., *Nonperturbative renormalization of composite operators in lattice QCD*, *Nucl.Phys.* **B544** (1999) 699–733, [hep-lat/9807044].

[34] G. M. von Hippel, B. Jger, T. D. Rae, and H. Wittig, *The Shape of Covariantly Smeared Sources in Lattice QCD*, *JHEP* **1309** (2013) 014, [arXiv:1306.1440].

[35] N. Cabibbo and E. Marinari, *A New Method for Updating SU(N) Matrices in Computer Simulations of Gauge Theories*, *Phys.Lett.* **B119** (1982) 387–390.

[36] F.-K. Guo, L. Liu, U.-G. Meissner, and P. Wang, *Tetraquarks, hadronic molecules, meson-meson scattering and disconnected contributions in lattice QCD*, *Phys.Rev.* **D88** (2013) 074506, [arXiv:1308.2545].

[37] **Particle Data Group** Collaboration, K. Olive et al., *Review of Particle Physics*, *Chin.Phys.* **C38** (2014) 090001.

[38] R. Sommer, *A New way to set the energy scale in lattice gauge theories and its applications to the static force and alpha-s in SU(2) Yang-Mills theory*, *Nucl.Phys.* **B411** (1994) 839–854, [hep-lat/9310022].

[39] Y. Chen, S.-J. Dong, T. Draper, I. Horvath, K.-F. Liu, N. Mathur, S. Tamhankar, C. Srinivasan, F. X. Lee, and J.-b. Zhang, *The Sequential empirical bayes method: An Adaptive constrained-curve fitting algorithm for lattice QCD*, hep-lat/0405001.